Chemical Engineering Journal 96 (2003) 45–54

Chemical Engineering Journal

www.elsevier.com/locate/cej

Hydrodynamics and mass transfer in a lab-scale three-phase internal loop airlift

Giuseppe Olivieri, Antonio Marzocchella*, Piero Salatino

Dipartimento di Ingegneria Chimica, Università degli Studi di Napoli Federico II, P.le V. Tecchio, 80-80125 Napoli, Italy

Abstract

The present paper addresses gas–liquid–solids hydrodynamic regimes that establish in a lab-scale internal circulation airlift operated at low superficial gas velocity batch-wise with respect to liquid and solid phases. Silica sand and glass beads have been used as bed solids at hold-up ranging between 4 and 12% by volume. Transition conditions between fixed bed, fluidized bed and solids circulation regimes have been assessed by means of analysis of pressure data, both in the time- and frequency-domains. Gas–liquid mass transfer coefficient and liquid circulation velocity have been measured in the fluidized bed and solids circulation regimes.

Keywords: Internal loop airlift; Regime transitions; Gas–liquid–solids system; Fluidization; Mass transfer

1. Introduction

The potential of gas–liquid–solids (GLS) fluidization technology in chemical and biochemical processes has been often addressed in the past decades [1–6]. A wide variety of contacting patterns, extensively described by Fan [6], can be selected depending on process requisites. Among the pneumatically agitated reactors the internal loop airlift is probably the most extensively used because of its intrinsically effective interphase mass transfer and moderate power consumption. The most common design is based on two coaxial cylinders with gas sparging either in the inner tube (draft) or in the annular region.

Hydrodynamic regimes of GLS systems in internal loop airlifts are strongly affected by solids and liquid properties as well as by reactor design. They have been classified into packed bed, fluidized bed and circulated bed regimes [6]. Research work has been mostly focused on the establishment of circulation regimes [7–13] while the onset of fluidized bed regime has received comparatively limited attention [8,14–16]. Flow regimes have been typically assessed by direct inspection of the bed and by analysis of time-averaged data. Time- and space-resolved measurements have been seldom adopted for the diagnosis of GLS flow [17–20], usually only for fluidized beds belonging to class E-1-a-1 according to Fan [6] classification.

Characterization of gas–liquid mass transfer rate and of liquid mixing in internal loop airlifts has also been frequently addressed in the literature. Chisti [5] comprehensively surveyed the subject pointing at the open issues and research priorities.

This work is part of a wider project aiming at analysing the effect of operating conditions (properties and loading of solids, superficial gas velocity, liquid flow rate) as well as reactor design (column size, location of gas sparger, bottom and top clearance, draft height) on hydrodynamics and interphase mass transfer in internal loop airlifts. The present paper reports on the assessment of hydrodynamic regimes in the operation of a lab-scale internal airlift equipped with a gas sparger located in the draft. Diagnostic tools and statistical and spectral data analysis procedures have been set up at the lab-scale. The performance of the system has been characterized in terms of: liquid circulation rate; analysis (both in the time- and frequency-domains) of the pressure time-series along the reactor; gas/liquid mass transfer coefficient. Experimental results have been directed to map hydrodynamic regimes, to characterize the dynamics of three-phase systems, to assess the effectiveness of interphase mass transfer.

2. Experimental

2.1. Apparatus

The experimental apparatus (Fig. 1) consists of a lab-scale internal loop airlift equipped with a gas flow controller, a

* Corresponding author. Tel.: +39-081-7682541;
fax: +39-081-5936936.
E-mail address: antonio.marzocchella@unina.it (A. Marzocchella).

1385-8947/$ – see front matter © 2003 Elsevier B.V. All rights reserved.
doi:10.1016/j.cej.2003.08.003

Nomenclature

A	cross-sectional area (m^2)
C_{O_2}	oxygen concentration in the liquid phase (g/m^3)
$C^*_{O_2}$	oxygen concentration in the liquid phase at equilibrium with the gas phase (g/m^3)
H	height (m)
$K_L a_L$	overall gas–liquid mass transfer coefficient referred to liquid phase (s^{-1})
K_p	friction loss coefficient (–)
P	pressure (Pa)
$\Delta P^{A–D}$	annulus–draft pressure difference (Pa)
t	time (s)
t_C	circulation time (s)
t_E	DOT probe response time (s)
U	superficial velocity (m/s)
z	axial coordinate (m)

Greek letters

ε	volume percentage (%)
ρ	density (kg/m^3)
σ_P^2	pressure variance (Pa^2)

Subscripts

C	circulating regime onset
F	fluidized regime onset
G, L, S	gas, liquid, solids phase

Superscripts

A, D	annulus, draft
Down	measurements carried out decreasing U_G
Up	measurements carried out increasing U_G

humidifier, diagnostic instrumentation and a data acquisition unit.

The lab-scale internal loop airlift is a 120 mm ID, 1.20 m high cylindrical column made of Plexiglas equipped with a coaxial 70/80 mm ID/OD, 0.53 m high Plexiglas draft tube. The bottom section of the external column has a conical shape characterized by a semi-angle of 56°. A vertical needle at the bottom of the draft is used to set the clearance for liquid circulation, fixed in the present study at 19 mm. The gas–liquid disengagement section is limited to the region just above the draft tube.

Both the cylindrical column and the draft tube are equipped with pressure taps connected to electronic pressure transducers. In particular 4 mm ID, 70 mm long pipes are used to connect hydraulically the draft tube taps to the transducers.

Gas was sparged in the draft tube by means of a multiple-orifice nozzle [21,22]. It consists of a vertical T-shaped device, made of 6 mm OD tube with six horizontal holes, 1 mm diameter, located along the horizontal branches (see inset of Fig. 1). Direct observation of gas sparging into

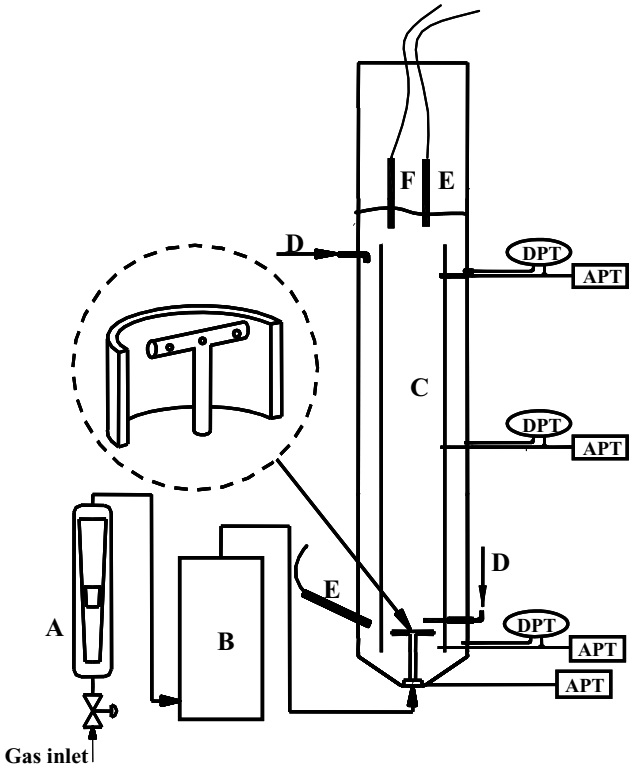

Fig. 1. The experimental apparatus: (A) flow meters; (B) humidifier; (C) internal airlift; (D) tracer injection probe; (E) pH probe; (F) DOT probe. DPT: differential pressure transducers APT-pressure transducer.

the liquid phase in the absence of solids confirmed that gas bubbles were uniformly distributed across the draft within a distance from the injection level equal to one diameter of the draft tube. The reactor design is such that the gas sparger can be located at different levels above the airlift bottom. In the actual configuration the sparger is located 40 mm above the airlift bottom.

The cylindrical column is equipped with several ports to insert probes into the apparatus. Ports are located mainly close to the bottom of the column and the section corresponding to the top of the draft tube. The humidifier consists of a 0.25 m ID, 0.50 m high column filled with 0.20 m water head.

2.2. Diagnostics

Visual inspection enabled qualitative and quantitative characterization of the hydrodynamic regime. In particular, gas hold-up was evaluated by measuring the liquid free-surface level.

Instrumentation consisted of broad-bandwidth relative pressure transducers, differential pressure transducers, a pH meter and a DOT meter.

Broad-bandwidth relative pressure transducers measured the pressure along the draft tube. Electronic differential pressure transducers measured the pressure difference between the draft tube and the annular region at the same level.

pH was measured by means of a probe (Broadley James) connected to a pH meter (Consort R305). The probe was connected directly to the data acquisition unit during liquid circulation velocity measurements.

Total dissolved oxygen was metered by means of a Clark electrode based DOT probe (Mettler Toledo, InPro 6050) connected to a DOT transmitter (Mettler Toledo, O_2 4100 Transmitter).

Signals from the pressure transducers were simultaneously recorded by a chart recorder and logged for 120 s at a sampling rate of 200 Hz on a PC equipped with a data acquisition card and low-pass analogic filters characterized by either 25 or 50 Hz cut-off frequencies. A Labview® data acquisition software was developed ad hoc.

Liquid circulation velocity was estimated by means of acid/base tracer technique based on the injection of a pulse of acid or base and time-resolved measurement of the pH downstream the injection point. The amount of injected acid or base and its concentration were fixed in order to have a finite difference in the ultimate pH value and to limit the increase of liquid hold-up. Runs were carried out injecting 5 ml of a 1 M solution of HCl or NaOH, corresponding to a change of two of pH. Injection and measurement point depended on the solids fluidization regime:

- no solids circulation regime—the pH probe was located at the bottom of the annulus and the tracer was injected at the top of the annulus;
- solids circulation regime—the pH probe was located at the top of the draft and the tracer injected just above the gas sparger.

Liquid phase was changed after every five acid/base tracer injections in order to keep the ionic strength close to the initial value of the tap water adopted.

Liquid superficial velocity in the draft (U_L^D) is calculated as:

$$U_L^D = \frac{H^D}{t_C}\left(1 + \frac{A^A}{A^D}\right) \quad (1)$$

where H^D is the draft height, A^A and A^D the cross-sectional area of the annulus and the draft respectively, t_C the time delay between successive peaks of the time-resolved pH measurement estimated by means of autocorrelation analysis. It has been assumed that equilibration of the carbonate/hydrogen-carbonate reaction is fast [23] compared with the liquid circulation time-scale. Accordingly, pH time-resolved measurements would be little affected as far as periodic fluctuations over the circulation time-scale are concerned.

Gas–liquid mass transfer coefficient was assessed by means of the transient technique [21,24]. At steady state gas stream was switched from air to nitrogen, or vice versa, and data from the DOT probe, located at the top of the reactor, were logged on the acquisition unit. Assuming the liquid phase well mixed, the oxygen concentration in the liquid phase (C_{O_2}) changes according to the relationship:

$$\frac{C^*_{O_2} - C_{O_2}(t)}{C^*_{O_2} - C_{O_2}|_{t=0}} = \left(\frac{e^{-tK_La_L}}{t_E} - K_La_L\, e^{-t/t_E}\right)\frac{t_E}{1 - t_E K_L a_L} \quad (2)$$

where K_La_L is the overall volumetric gas–liquid mass transfer coefficient referred to the liquid unit volume, $C^*_{O_2}$ the oxygen concentration in equilibrium with the gas phase and t_E the DOT probe response time. Following the procedure suggested by Chisti [21], time-resolved DOT data have been worked out and reported as $\ln[(C^*_{O_2} - C_{O_2}(t))/(C^*_{O_2} - C_{O_2}|_{t=0})]$ vs. t plot. The value of K_La_L has been estimated as the slope of the plot. Only data points corresponding to times longer than the DOT probe response time (about 60 s) were considered to this purpose.

2.3. Materials

The plant was operated batch-wise with respect to the water and solids. Air was continuously fed to the column during operation.

The liquid phase consisted of 5.4 l of tap water at room temperature. This loading corresponded to a top clearance of 10 mm under gas-free conditions.

Table 1 reports the properties of the solids tested. Most of the experiments were carried out using silica sand particles of average diameter equal to 175 μm. For comparison purposes glass beads were tested as well. Glass beads and silica sand differed as regard sphericity and particle roughness. In particular glass beads were much smoother, as can be inferred by the lower angle of repose in air reported in Table 1 [26]. Solids hold-up was varied between 0.2 and 0.6 l, corresponding to a gas-free volume fraction (ε_S) spanning between 4 and 12%.

2.4. Procedure

Once the solids hold-up was fixed, the gas superficial velocity (U_G—based on the cross-sectional area of the column)

Table 1
Properties of solids tested

Material	Glass beads	Silica sand
Sauter mean diameter (μm)	175	175
Size range (μm)	150–200	150–200
Sphericity (–)	≈1	0.8
Particle density (kg/m^3)	2540	2600
Angle of repose in air (°)	20	32
Terminal velocity[a] (m/s)	0.019	0.018
Minimum liquid fluidization velocity[b] (m/s)	2.7×10^{-3}	2.8×10^{-3}

[a] Value calculated according to Haider and Levenspiel [25].
[b] Value calculated under mode E-1-a-1 fluidized bed according to Fan [6].

was increased from zero up to a maximum value that was limited by one of the following constraints: (i) the maximum expansion of the GLS system compatible with present configuration of the plant (fluidization column = 1.20 m); (ii) the maximum admissible over-pressure in the plant upstream the gas sparger. Steadiness of operation was continuously monitored by recording the pressure at the draft bottom with a chart recorder.

Under each set of operating conditions the behaviour of the airlift was characterized by the following techniques: (1) visual inspection of the system, including continuous recording of water height vs. U_G; (2) time-resolved recording of the pressure profile along the loop, at different values of U_G.

Time-series of measured variables were eventually worked out to yield statistical and spectral parameters. In particular the average and the variance of the time-series were adopted in the present work to mark singularities associated with fluidization regime transitions. Liquid velocity and gas–liquid mass transfer coefficient were estimated under selected operating conditions.

3. Results and discussion

3.1. Analysis of time-averaged pressure

Fig. 2 reports the time-averaged values of the following variables: (a) pressure measured along the draft (relative to hydrostatic pressure measured with the same liquid and solids loading but with no gas feeding) (Fig. 2A); (b) differential pressure between the draft and the annulus (at a given level) (Fig. 2B); (c) overall gas hold-up and bubble penetration depth in the annular zone (Annulus Bubble Depth—ABD) (Fig. 2D). Data were recorded during runs carried out with 175 μm silica sand ($\varepsilon_S = 8\%$) at different gas superficial velocities U_G in the range between 0 and 5.5 cm/s. Data points collected in tests carried out with either increasing (closed symbols) or decreasing (empty symbols) values of U_G are reported. Analysis of data points in Fig. 2 and of the phenomenology at different values of U_G suggests the existence of three distinct hydrodynamic regimes. Transitions between regimes were identified from discontinuities of either the value or of the slope of draft pressure and/or annulus–draft differential pressure (ΔP^{A-D}) vs. U_G plots.

- Regime I, $U_G < U_{G,F}^{Up} = 2.6$ cm/s: pressure in the draft decreases steadily as U_G increase at all pressure taps with the exception of those located close the top of the draft: at this level the pressure is relatively steady. The annulus–draft differential pressure increases with U_G at any level, and so does gas hold-up. No bubble penetration is observed in the annulus. A fixed bed of solids whose height increases with U_G is established in the annular region.
- Regime II, $U_{G,F}^{Up} < U_G < U_{G,C}^{Up} = 2.9$ cm/s: the pressure in the draft is nearly constant and ΔP^{A-D} slightly increases with U_G whatever the pressure tap level. No bubble penetration is observed in the annulus. Gas hold-up increases steadily with U_G. Solid particles are elutriated from the draft, to settle down eventually in the annular region where packed bed moving downward at a velocity of about 1 mm/s can be observed.
- Regime III, $U_{G,C}^{Up} < U_G$: the pressure at the bottom of the draft ($z = 0$ cm) and ΔP^{A-D} increases almost stepwise at $U_G = U_{G,C}^{Up}$ to remain relatively constant thereafter. The higher the level in the bed, the larger the stepwise change of pressure in the draft. Further increase of U_G is associated with decreasing ($z = 4.5$ cm) or increasing ($z = 26.3$ and 41.2 cm) values of the draft pressure depending on the measurement level. Bubble penetration depth and gas hold-up increase with U_G.

Similar hydrodynamic regimes were outlined by Fan et al. [8]. When the gas superficial velocity is decreased, hysteresis cycles become evident in all the plots of Fig. 2, similarly to what documented by Heck and Onken [14]. Moreover, direct transition from Regime III to Regime I is observed, and Regime II is not established in between. $U_{G,C}^{Down} = 2.1$ cm/s, the value at which sharp decrease of draft pressure and increase of differential annulus–draft pressure is observed, marks the transition from circulation regime directly to fixed bed conditions.

The pressure profile recorded at the draft bottom ($z = 0.2$ cm) at U_G larger than 2.6 cm/s resembles those obtained by previous investigators [7,14].

Fig. 3A–E reports the pressure loops across the draft and the annular regions recorded at different values of the gas superficial velocity. Fig. 3A and B refer to the fixed bed regime: the pressure in the upper annulus is fairly constant and its value is determined by the increase of the water free-surface level associated with gas feeding. Pressure measured at the bottom of the annular region ($z = 4.5$ cm) is smaller than those measured at the other taps up in the annular region. This feature, together with the observation that gas bubbles are absent in the annulus under these conditions, indicates that a fixed bed is established at the level ($z = 4.5$ cm) of the lowest pressure tap in the annulus. Liquid flow through the fixed bed of solids is driven by the pressure drop across the annulus and, further on, by the pressure drop across the draft clearance. Moving up along the column axis, the pressure increases in the draft more rapidly than in the annulus until a crossover between the two pressure profiles is observed at levels very close to the bed surface.

Fig. 3C refers to operation in the Regime II: the pressure along the draft is not remarkably affected by changing U_G within the range of gas superficial velocities corresponding to this regime. The pressure in the annulus moderately increases as a consequence of solids entrained in this region.

Fig. 3D and E refer to operation in the circulation regime (Regime III). As soon as the threshold value $U_{G,C}^{Up}$ is approached the shape of the pressure loop changes drastically. Pressure increases in both the draft and the annular

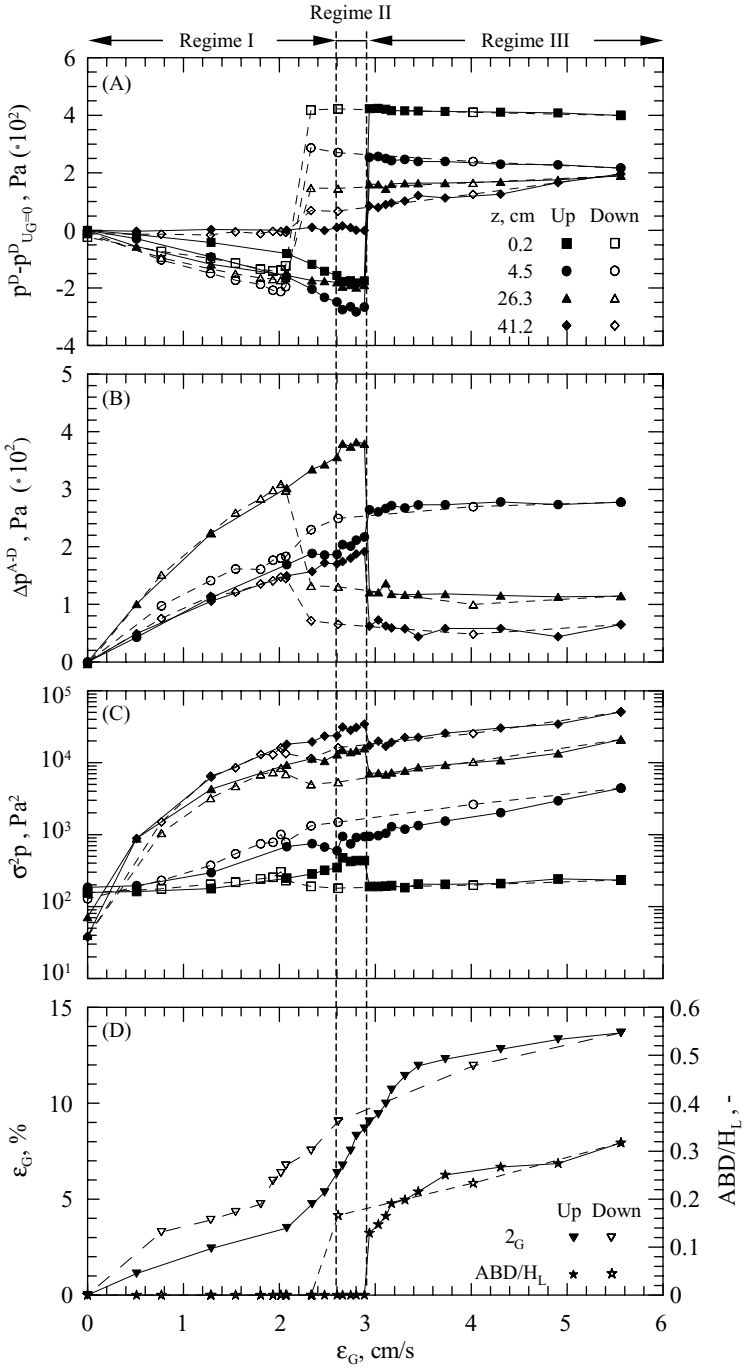

Fig. 2. Time-averaged variables measured at different gas superficial velocities. Axial pressure along the draft (A), differential draft–annulus pressure (B), variance of the draft pressure (C) and dimensionless bubble penetration depth and gas hold-up (D). Empty symbols refer to measurements carried out at decreasing velocity. Bed material: 175 μm silica sand, $\varepsilon_S = 8\%$.

regions, compared with the hydrostatic value, due to the presence of the suspended solids in the flow. Pressure increases steadily when moving from the top to the bottom, both in the draft and in the annulus. This increase is less pronounced at the highest value of U_G (Fig. 3E) than at the lowest one (Fig. 3D), due to the larger gas hold-up associated with larger U_G. Under these conditions, gas bubbles are no more confined into the draft region but extend well into the upper annular zone (see also the bubble penetration depth in Fig. 2D).

In the circulating regime, pressures measured at the bottom of the draft and of the annulus may be related to the solids hold-up. The pressure drop across a fluidized suspension equals the buoyant weight of the solids per unit cross-sectional area of the column, provided that the momentum flux related to gas injection can be neglected

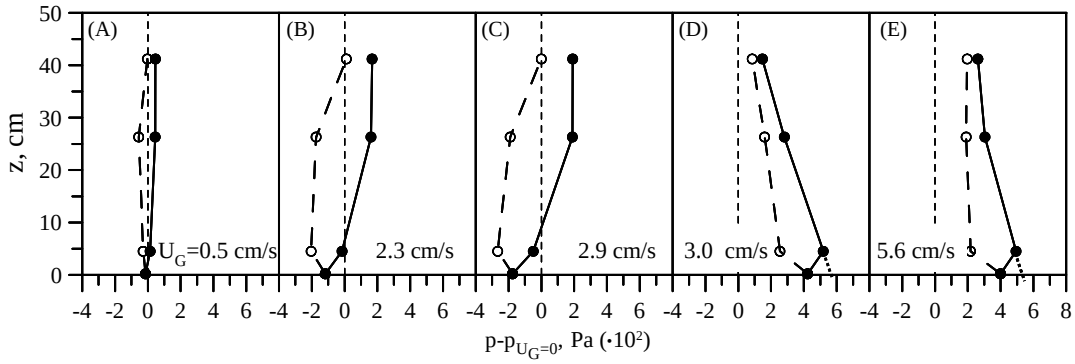

Fig. 3. Pressure loop in the airlift measured at different gas superficial velocities. Bed material: 175 μm silica sand, $\varepsilon_S = 8\%$. Closed symbols refer to the annulus, empty symbols to the draft.

[27]. The annulus pressure—relative to hydrostatic value—extrapolated to the bottom of the vessel to account for the hydrostatic head is 5.5×10^2 Pa (Fig. 3D and E). This figure compares well with that (5.7×10^2 Pa) calculated under the assumptions—which are fairly well satisfied in the circulation regime—that solids in the annulus are fluidized and that their loading equals the average hold-up in the column ($\varepsilon_S = 8\%$). The difference between the extrapolated pressure and the one measured at the bottom of the vessel (4.2×10^2 Pa) provides the driving force for the circulation flow across the draft clearance.

3.2. Influence of solids hold-up and solids properties on regime transition velocities

Fig. 4 reports the regime transition velocities as a function of the solids hold-up measured under gas-free conditions (ε_S) for the water–175 μm silica sand system and for 175 μm glass beads. In general, all regime transitions occur at velocities that increase as ε_S increases. It is noteworthy that the hysteresis range $U_{G,C}^{Up}$–$U_{G,C}^{Down}$ is very narrow for ε_S smaller than about 8%. For ε_S larger than this figure the hysteresis range becomes progressively broader, mostly because of a rather steep increase of $U_{G,C}^{Up}$ as ε_S departs from 8%.

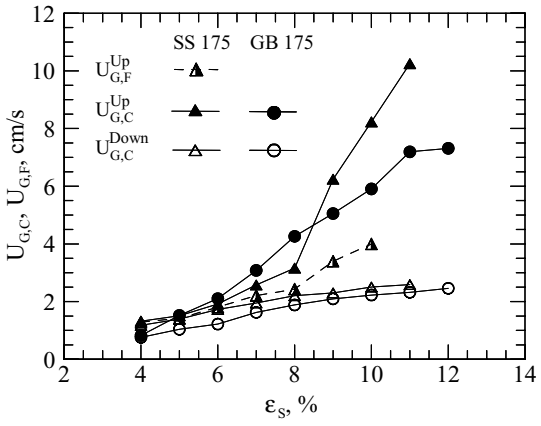

Fig. 4. Regime transition velocities as a function of solids hold-up for different bed solids.

The comparison with data measured with different bed solids provides some insight into the factors which influence the behaviour of the systems at hand. Transitions between Regimes I and II have not been estimated during runs carried out with glass beads while the attention was focused on the transition to circulation regime. It can be noted that the glass beads, unlike being of the same density and size as the silica sand, have generally lower regime transition velocities that gradually increase with ε_S. Altogether, it may be inferred that particle roughness and/or sphericity play a key role in determining the value of U_G at the transition between regimes as well as the breadth of the hysteresis range. It is likely that parameters like the angle of internal friction and the angle of wall friction of the granular material be relevant to the hydrodynamic regime.

3.3. Analysis of pressure time-series in the time- and frequency-domains

Other important features of the hydrodynamic regimes can be recognized with the aid of time- and frequency-domain analysis of the pressure time-series.

Fig. 2C reports the variance of the pressure signal (σ_p^2) recorded in the draft as a function of U_G in runs carried out with 175 μm silica sand ($\varepsilon_S = 8\%$). The variance increases when moving from the bottom to the top of the draft. The variance increases as U_G increases throughout the range investigated, with the exception of a sharp stepwise decrease of σ_p^2 as U_G becomes larger than $U_{G,C}$. Noteworthy, this stepwise change is not observed at the pressure tap located immediately below the gas sparger, $z = 4.5$ cm.

Fluctuations of pressure can be interpreted as a consequence of dynamic perturbations imparted to the bed by bubble bursting at the bed surface [17]. Accordingly, the variance of the pressure time-series can be assumed as a measure of how finely is gas dispersed as bubbles in the

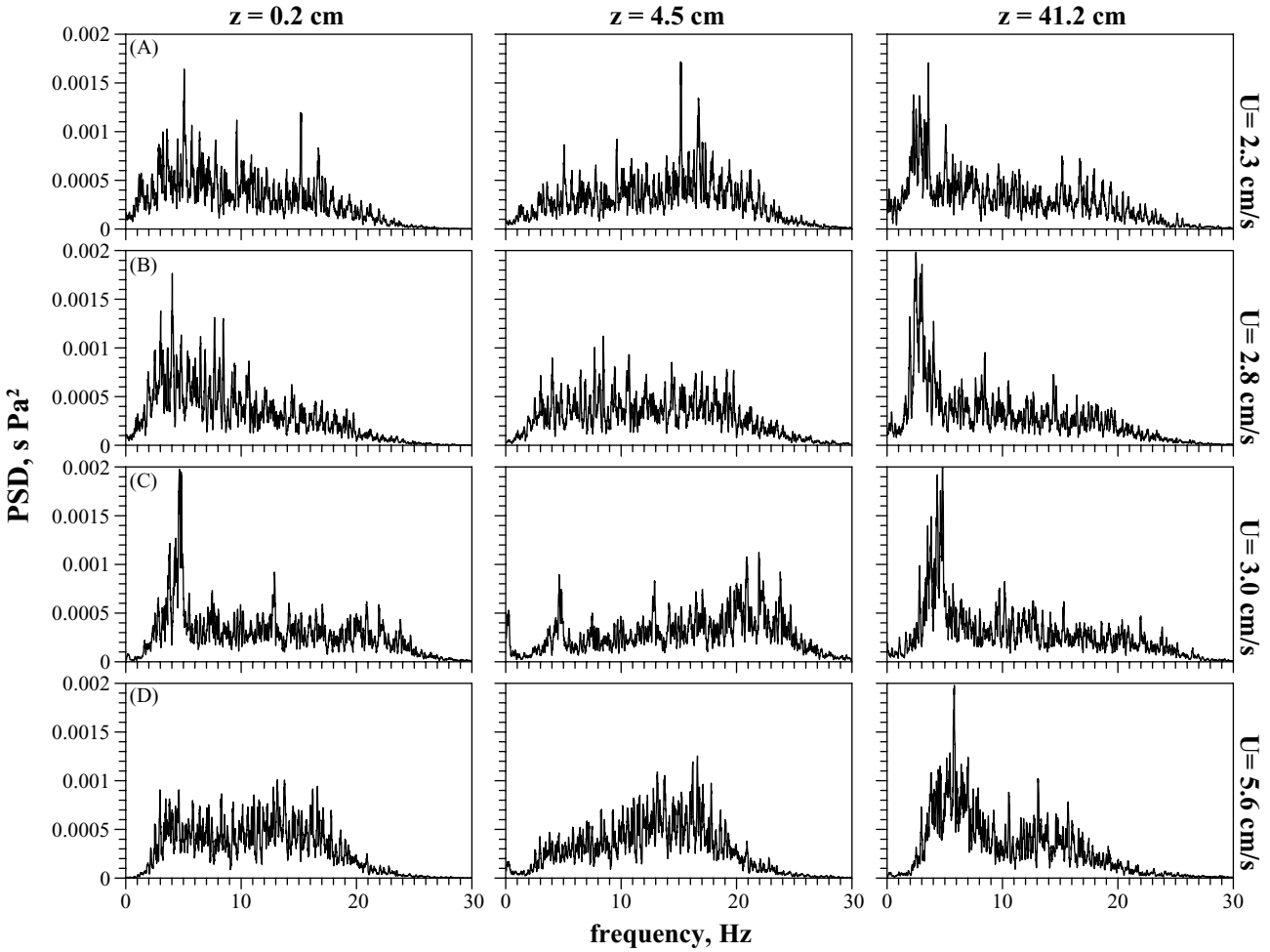

Fig. 5. PSD of time-series of the draft pressure at different gas superficial velocities and measurement levels. Bed material: 175 μm silica sand, $\varepsilon_S = 8\%$: (A) fixed bed regime; (B) fluidized bed regime; (C) onset of solids circulation regime; (D) developed solids circulation regime.

suspension. Consistently with the relationship between variance of pressure and mean bubble size established by Fan et al. [17], the sudden decrease of the variance at the onset of the circulation regime corresponds to the establishment of a more finely dispersed gas phase, most likely associated with the cocurrent flow patterns of the liquid and of the gas phase in the draft tube.

Frequency-domain analysis of the time-series of pressure recorded in the draft has been carried out to obtain the power spectral density (PSD) of the signal. Selected plots of PSD corresponding to different hydrodynamic regimes and different pressure tap levels are reported in Fig. 5. The following features can be recognized in the PSD function of pressure fluctuations measured at the draft bottom ($z = 0.2$ cm):

(A) Fixed bed regime—a wide spectrum of periodic phenomena (frequency ranging between 1 and 25 Hz) has been observed. A dominant peak corresponding to about 4–5 Hz and smaller peaks at lower and higher frequencies can also be recognized.

(B) Regime II—periodic phenomena characterized by frequencies of about 4 Hz become progressively more evident.

(C) Regime III onset—as the circulation regime establishes, dominant frequencies suddenly appear located between 4 and 5 Hz.

(D) Full-developed Regime III—no dominant frequency is observed. The bandwidth of the frequency spectrum reduces.

PSD functions estimated from time-series recorded at different locations along the riser–4.5 cm (just below the gas sparger) and 41.2 cm–differ from those estimated at the draft bottom mainly as regards (Regimes II and III). Within Regime I operating conditions, frequencies corresponding to dominant peaks are barely affected by the recording level, whereas remarkable changes of the relative power along the draft are observed. Under Regime II, no dominant frequency is recorded just below the gas sparger while a strong peak is observed at the draft top at about 2–3 Hz. At larger gas velocity (Regime

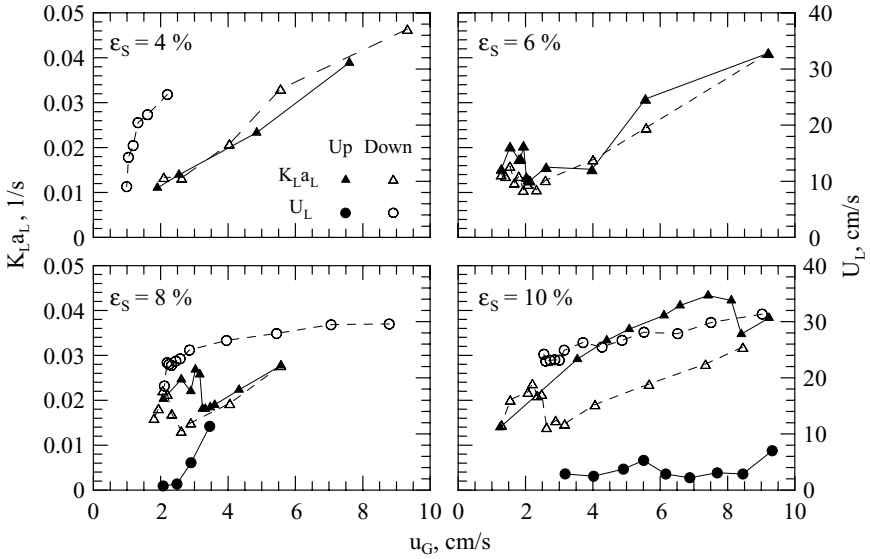

Fig. 6. Liquid circulation velocity and gas–liquid mass transfer coefficient as a function of gas superficial velocity for different hold-up of bed solids. Bed material: 175 μm silica sand.

III) a strong peak—5–6 Hz—is observed at the draft top.

The sharp increase of the dominant frequency observed at the draft top ($z = 41.2$ cm) moving from fluidized bed to the circulation regime is consistent with the observation that a more finely dispersed bubble phase is established in the latter regime, characterized by cocurrent flow of all the phases. At the onset of the circulation regime gas flow rate is approximately equal to that fed under fluidized bed regime, therefore an increase of the dominant frequency—corresponding to an increase of number of bubbles bursting at the bed surface per unit time—implies a reduction of the average bubble size.

3.4. The liquid circulation velocity

Fig. 6 reports the liquid circulation velocity (U_L^D) relative to different 175 μm silica sand hold-up estimated as reported in Section 2.2. Liquid circulation velocities are in the order of 0.2–0.3 m/s in the fully developed circulation regime and, as expected [12], rather insensitive to the value of the U_G. It is likely that the pressure drop across the draft clearance and the head above the clearance itself be the variables controlling the circulation velocity.

In the fixed bed regime much smaller circulation velocity, in the order of 0.03 m/s, are recorded. Assessment of U_L^D in the fixed bed regime may be seriously affected by tracer diffusive phenomena: smoothing out of pH time-fluctuations may reduce the accuracy of measurements of the circulation time.

In the fluidized bed regime U_L^D increases with U_G.

Data of U_L^D in the circulation regime have been worked out, together with data concerning pressure drop at the airlift bottom (ΔP), to calculate the friction loss coefficient (K_p) relative to the 180° annulus-to-draft bend, according to the relationship:

$$\Delta P = K_p[\tfrac{1}{2}\rho^*(U_L^D)^2] \quad (3)$$

where ρ^* is the solids–liquid pseudo-homogeneous phase density estimated neglecting the gas contribution as $[\rho_L(1 - \varepsilon_S) + \rho_S\varepsilon_S]$, ρ_L and ρ_S being, respectively, the liquid and the solids density.

From the ΔP^{A-D} measured at 4.5 cm (1.5 cm above the draft edge) and the U_L^D measured in the fully circulating regime ($U_G \gg U_{G,C}$), K_p is computed to be between 4.2 and 5.3 with 175 μm silica sand at ε_S ranging between 4 and 10%. This range of values is in good agreement with previous measurements [10,12] and about one order of magnitude larger than values predicted for homogeneous liquid phase [28].

3.5. Gas–liquid mass transfer coefficient

Fig. 6 reports the overall gas–liquid mass transfer coefficient (K_La_L) as a function of U_G measured during runs carried out with 175 μm silica sand at different ε_S. Data were reported only for operating conditions characterized by mass transfer time-scale at least 5–6 times larger than the circulation time-scale in order to fulfil the assumption that the liquid phase was well mixed.

Analysis of the figure suggests that K_La_L increases steadily with U_G with the exception of a stepwise decrease occurring at the transition to the circulation regime. Dependence of K_La_L on U_G is moderate throughout the circulation regime range. The effect of ε_S on K_La_L is negligible, both in the fixed bed and in the solids circulation regimes, under the operating conditions tested. Gas–liquid mass transfer is apparently governed by the gas flow rate. The ε_S af-

fects $K_L a_L$ only through the influence it exerts on the fixed bed/fluidized bed/circulating bed regime transitions.

The sharp decrease of $K_L a_L$ associated with the onset of the circulation regime remains to be explained. On the one hand, the above recalled establishment of finer gas bubble dispersion in the circulation regime should favour the increase of gas–liquid interfacial area. On the other hand the cocurrent motion of gas, liquid and solid phases in the circulation regime might negatively affect gas–liquid mass transfer rate. Further experimental evidence is needed to fully assess the relative importance of these processes.

4. Conclusions

A lab-scale internal loop airlift reactor has been operated under conditions ranging from fixed bed to solids circulation regimes, batch-wise with respect to the liquid and the solid phases. Flow regimes, namely fixed bed, fluidized non-circulating and circulating regimes, have been mapped as a function of gas superficial velocity, and solids hold-up and properties. Time-series of pressure data have been analysed both in the time- and frequency-domains. The variance of the pressure and its PSD turn out to be sensitive to changes in the hydrodynamic regime and provide a reliable tool for regime assessment also for GLS internal loop airlifts.

Gas superficial velocities at the threshold between hydrodynamic regimes depend on whether gas superficial velocity is being increased or decreased, therefore hysteresis cycles are observed.

Particles roughness and/or particles shape turn out to be relevant to regime transitions. As particle roughness increases and/or particles shape departs from spherical: (i) the onset of circulation regime as superficial gas velocity is increased is delayed; (ii) the hysteresis cycle broadens. The importance of particle roughness/shape is emphasized as the solids hold-up is increased.

Liquid circulation velocity has been reported as a function of the gas superficial velocity and solids hold-up. It is barely dependent on the solids hold-up, apart for the influence that this variable exerts on the establishment of the hydrodynamic regimes observed.

The overall gas–liquid mass transfer coefficient is characterized by a moderate dependence on solids hold-up. It generally increases as the gas superficial velocity increases, except when the system approaches the threshold for the onset of the circulation regime: a nearly stepwise decrease of the gas–liquid mass transfer rate is observed on the verge of the circulating regime.

Acknowledgements

The support of Miss Margherita Ponticelli in the experimental campaign is gratefully acknowledged. Financial support from MIUR within the framework of the research program on “Multiphase systems for granular solids treatment and multiphase reactors in the process industry” is acknowledged.

References

[1] G. Volpicelli, L. Massimilla, Three-phase fluidized bed reactors: an application to the production of calcium bisulphite acid solutions, Chem. Eng. Sci. 25 (1970) 1361–1373.
[2] M.H. Siegel, C.W. Robinson, Applications of airlift gas–liquid–solid reactors in biotechnology, Chem. Eng. Sci. 47 (13/14) (1992) 3215–3229.
[3] F. Gòdia, C. Solà, Fluidized-bed bioreactors, Biotechnol. Prog. 11 (1995) 479–497.
[4] K. Schugerl, Three-phase-biofluidization—application of three-phase fluidization in the biotechnology—a review, Chem. Eng. Sci. 57 (21/22) (1997) 3661–3668.
[5] Y. Chisti, Pneumatically agitated bioreactors in industrial and environmental bioprocessing: hydrodynamics, hydraulics and transport phenomena, Appl. Mech. Rev. 51 (1) (1998) 33–98.
[6] L.-S. Fan, Gas–Liquid–Solid Fluidization Engineering, Buttherwoths, Stoneham, MA, 1989.
[7] K. Koide, K. Horibe, H. Kawabata, S. Ito, Critical gas velocity required for complete suspension of solid particles in solid-suspended bubble column with draught tube, J. Chem. Eng. Jpn. 17 (4) (1984) 368–374.
[8] L.-S. Fan, S.-J. Hwang, A. Matsura, Hydrodynamic behaviour of a draft tube gas–liquid–solid spouted bed, Chem. Eng. Sci. 39 (12) (1984) 1677–1688.
[9] M. Immich, U. Onken, Prediction of minimum gas velocity in suspended bubble columns and airlift reactors, Chem. Eng. Sci. 47 (13/14) (1992) 3379–3386.
[10] A.G. Livingston, S.F. Zhang, Hydrodynamic behaviour of three-phase (gas–liquid–solid) airlift reactor, Chem. Eng. Sci. 48 (9) (1993) 1641–1654.
[11] S.-J. Hwang, Y.-L. Cheng, Gas holdup and liquid velocity in three phase internal-loop airlift reactors, Chem. Eng. Sci. 52 (21/22) (1997) 3949–3960.
[12] J.J. Heijnen, J. Hols, R.G.J.M. van der Lans, H.L.J.M. van Leeuwen, A. Mulder, R. Weltrede, A simple hydrodynamic model for the liquid circulation velocity in a full-scale two- and three-phase internal airlift reactor operating in the gas recirculation regime, Chem. Eng. Sci. 52 (15) (1997) 2527–2540.
[13] H. Kojima, J. Sawai, H. Uchino, T. Ichige, Liquid circulation and critical gas velocity in slurry bubble column with short size draft tube, Chem. Eng. Sci. 54 (1999) 5181–5185.
[14] J. Heck, U. Onken, Hysteresis effects in suspended solid particles in bubble column with and without draft tube, Chem. Eng. Sci. 42 (5) (1987) 1211–1212.
[15] D. Pošarac, D. Petrović, An experimental study of the minimum fluidization velocity in a three-phase external-loop air-lift reactor, Chem. Eng. Sci. 43 (5) (1988) 1161–1165.
[16] D. Petrović, D. Pošarac, A. Duduković, D. Skala, Minimum fluidization velocity of large particles in a draft tube airlift reactor, Chem. Eng. Sci. 48 (4) (1993) 2663–2667.
[17] L.-S. Fan, S. Satija, K. Wisecarver, Pressure measurements and flow regime transitions in gas–liquid–solid fluidized beds, AIChE J. 32 (1986) 338–340.
[18] K. Kitano, K. Ikeda, Flow regime of three phase fluidized bed, in: K. Yoshida, S. Morooka (Eds.), Proceedings of the Asian Conference on Fluidized-bed and Three-phase Reactors, Sanjo-Kaikan, 1988, pp. 361–367.
[19] C.M. Van den Bleek, M.-O. Coppens, J.C. Schouten, Application of chaos analysis to multiphase reactors, Chem. Eng. Sci. 27 (2002) 4763–4778.

[20] C. Boyer, A. Duquenne, G. Wild, Measuring techniques in gas–liquid and gas–liquid–solid reactors, Chem. Eng. Sci. 57 (2002) 3125–3185.
[21] Y. Chisti, Airlift Bioreactors, Elsevier, London, 1989.
[22] C. Vial, E. Camarasa, S. Poncin, G. Wild, N. Midoux, J. Bouillard, Study of hydrodynamic behaviour in bubble columns and external loop airlift reactors through analysis of pressure fluctuations, Chem. Eng. Sci. 55 (2000) 2957–2973.
[23] C.H. Bamford, C.F.H. Tipper, Comprehensive Chemical Kinetics, vol. 6, Reaction of Non-metallic Inorganic Compounds, Elsevier, Amsterdam, 1972.
[24] J.E. Bailey, D.F. Ollis, Biochemical Engineering Fundamentals, McGraw-Hill, Singapore, 1986.
[25] A. Haider, O. Levenspiel, Drag coefficient and terminal velocity of spherical and nonspherical particles, Powder Technol. 58 (1989) 63–70.
[26] H.J. Hermann, Granular matter, Physica A 313 (2002) 188–210.
[27] J.P. Couderc, Incipient fluidization and particulate system, in: J.F. Davidson, J.F. Clift, R. Harrison (Eds.), Fluidization, 2nd ed., Plenum Press, New York, 1985, pp. 1–46.
[28] D.S. Miller, Internal Flow Systems, BHRA Fluid Engineering, British Library Cataloguing, 1978.